Aerospace Science and Technology, Volume 121, February 2022, Article number 107284
DOI: 10.1016/j.ast.2021.107284

Identification of the key design inputs for the FEM-based preliminary sizing and mass estimation of a civil aircraft wing box structure

C. You [a,b], M. Yasaee [a*], S. He [a], D. Yang [a], Y. Xu [a], I. Dayyani [a], H. Ghasemnejad [a], S. Guo [a], P. Webb [a], J. Jennings [c], G. Federico [c]

[a] School of Aerospace, Transport and Manufacturing, Cranfield University, UK

[b] College of Energy and Power Engineering, Nanjing University of Aeronautics and Astronautics, Nanjing 210016, China

[c] Rolls-Royce plc, Derby, UK

Abstract

FEM-based preliminary structural sizing has been successfully carried out for a typical single-aisle wing box structure using MSC Nastran, by considering various load cases representing typical aircraft manoeuvres, engine loads, landing and ground handling conditions. The strength, buckling and fatigue criteria have been applied as the design constraints for sizing. The resultant total mass and the structural (static and modal) behaviour of the sized wing box model have been verified against a validated high-fidelity wing box model. A sensitivity analysis has been performed to evaluate the influence of the number of design fields and the selected design inputs (i.e. load cases and design constraints) on the accuracy of sizing and mass estimation of the wing box. This sensitivity analysis has also been extended to the static and modal behaviour of the wing box structure obtained from sizing. It provides an insight into the significance of considering the buckling and fatigue constraints, aircraft rolling loads, engine loads and landing loads in sizing, in addition to the commonly-applied 2.5g aircraft pull-up loads under the strength constraint. The findings of this study highlight the trade-off between the sizing efficiency and accuracy of a civil aircraft wing for modelling purposes.

Keywords: Wing mass estimation; Wing box sizing; Finite element model; Aircraft loads; Structural analysis

1. Introduction

1.1. Classification of wing structural sizing

The structural design of a wing is usually determined by multidisciplinary criteria (e.g. strength, fatigue, buckling, flutter, etc.). The sizing design is expected to find an optimum solution (e.g. minimum weight or cost) satisfying numerous requirements being associated with the criteria under critical load cases. This is done by adjusting the thickness distribution of each structural component of the wing (i.e. top & bottom skins with attached stringers, front & rear spars and ribs) for a given structural layout [1].

* Corresponding author.
Email address: M.Yasaee@cranfield.ac.uk (M. Yasaee)

Published by Elsevier. This is the Author Accepted Manuscript issued with: Creative Commons Attribution Non-Commercial No Derivatives License (CC:BY:NC:ND 4.0).
The final published version (version of record) is available online at DOI:10.1016/j.ast.2021.107284. Please refer to any applicable publisher terms of use.

The conventional sizing and the associated mass estimation of a civil aircraft wing can be classified into three stages – rapid, preliminary and detailed sizing, which are linked to the three main phases of aircraft design (i.e. conceptual, preliminary and detailed design) [2, 3].

Rapid sizing is usually involved in the aircraft conceptual design phase, which focuses on the global aircraft behaviour and the corresponding stiffness requirements in cooperation with flight physics. The word “rapid” refers to its spirit of keeping but speeding up the sizing optimisation process compared to the preliminary and detailed sizing. During rapid sizing, a global FE model, typically beam elements only, is usually applied to represent the real wing [4, 5]. Simple stress sizing (based on simplified engineering equations) can be carried out for the beam cross section geometry to provide sizing and global mass distribution without necessarily implementing detailed stress analysis. Multidisciplinary optimisation (e.g. the stress and flutter optimisation chain) can be efficiently conducted at this design phase to provide multidisciplinary analysis on the trade-offs, due to high computing efficiency of the beam model [3-5].

Preliminary sizing is the subsequent sizing process with higher fidelity, which is usually carried out at the aircraft preliminary design phase, based on a more realistic FE model displaying the explicit structural layout of the wing box, but with some detailed structural features being omitted (e.g. stiffeners, cutouts, joints, etc.) [3, 6]. More advanced sizing criteria (e.g. more explicit strength and buckling criteria) are applied at this stage to address the redistribution of internal loads, and to consolidate the sizing before finer studies, providing more accurate mass estimation than the first stage [2]. However, the updated sizing results are rarely fed back to the first stage in the conventional procedure, which impedes optimal design target satisfying stiffness and stress requirements simultaneously. To overcome this limitation, the recent trend is integrating the rapid and preliminary sizing stages with iterations allowed between them [2, 4, 7-9], such as the COMBOX tool applied by Airbus in A350 design [2]. Another recent trend is to combine the sizing process with topology optimisation to further explore the potential in weight saving[10, 11]. Stanford et al. [12, 13] proposed a two-level optimisation algorithm to improve the efficiency of optimisation, where structural layout and panel thickness distributions are optimised in the first and second level respectively.

At the phase of aircraft detailed design, detailed sizing of each part is conducted with fixed external loads (at the part level) determined from preliminary design, dealing with detailed design of all structural parts down to system brackets for example. Locally refined FE models containing all relevant details of the design are usually required at this phase. Some particular local design criteria (e.g. reparability and damage tolerance) may also need to be considered for detailed sizing. Load redistribution within the part is usually allowed to ensure that the structural sizing requirements are satisfied both globally and locally.

1.2. Design load cases and constraints applied in wing structural sizing

To obtain reasonable sizing results, the considered load cases need to sufficiently represent the most critical loading conditions experienced during flight. The aerodynamic loads being associated with the 2.5g symmetric pull-up manoeuvre are normally regarded as the most critical load case for a civil aircraft wing in terms of the load factor, hence have been considered as the dominant load case in most of the published sizing work [4, 5, 7, 14-21]. However, some other manoeuvres may result in localised higher loads which are not covered by the 2.5g loads mentioned above. Therefore, various other load cases representing the aerodynamic loads for cruise flight [7, 16], push-down manoeuvre [15, 16, 19, 20, 22], rolling manoeuvre [4, 5, 12], landing (with flaps in landing configuration) [16], gust [5, 16, 23-25], etc. have also been considered as design load cases in some studies. In addition to aerodynamic loads, localised load cases such as engine manoeuvre loads, landing gear loads, hydrostatic fuel loads, etc. have been taken into account in [11, 16, 25, 26] to increase the fidelity of the driving load cases for sizing.

Design constraint is also a key factor affecting the reliability of the sizing results. For a wing box structure, the predominant constraints are strength and buckling requirements based on stress analysis, which is performed at each structural component to ensure the structural integrity under the given design load cases [3-5, 7, 8, 14, 15, 19, 20, 23]. Fatigue constraint is also necessary for sizing the bottom skin considering the cyclic tensile load experienced during flight [3, 27, 28]. Another type of constraints that has been applied in some publications is the aeroelastic requirements regarding aileron effectiveness and flutter speed, which is beyond the scope of stress analysis and normally requires significant additional efforts to find feasible solutions [3, 4, 12, 23, 29]. In addition, some manufacturing requirements have also been applied as design constraints, such as the minimum stringer thickness to height ratio [3], and stacking sequence rules for composite parts [8, 13, 15, 19, 20, 25].

1.3. Recent development of wing structural sizing methods

Grihon et al. [2, 30] provided a review of the sizing methods that have been applied in Airbus, representing the typical development of the structural sizing of wing. During the early years, wing sizing was implemented mainly using iterative resizing loops, which was guided by engineer experience. This approach is still being used today to provide quick initial sizing. Building on this approach, the numerical optimisations minimising the total structural mass was developed, relying on gradient-based optimisation methods. To facilitate the sizing process, the optimisation capabilities have been built into some in-house and commercial FE packages, among which Nastran SOL200 is the most widely used one, where the structural responses from FE or engineering equations can be conveniently used during the optimisation [3, 4, 17, 20, 31]. In addition, some more complex analytical (semi-analytical) stress tools, with running times much less than FE calculation, were also developed [32]. These tools usually contain a long list of chained equations that are too complex to be integrated in Nastran SOL200, but can be linked with some open optimisation frameworks to improve the optimisation efficiency. A

typical example is the weight saving campaign made for A380, where some stiffened panels were optimised using the integrated stress tools in BOSS Quattro [2, 33].

There has also been a trend to use parametric CAD/CAE models in preliminary sizing to achieve an automatic high-fidelity design process, which has been particularly beneficial for improving the sizing efficiency [8, 9, 14, 16, 17, 21, 27, 29, 31, 34, 35]. Each component of the wing is discretised into numerous patches according to the given structural layout, where local sizing can then be carried out. Bindolino et al. [4] and Dababneh et al. [36] investigated the influence of the fidelity level of the applied wing box FE model on the sizing and mass estimation results. They recommended that a wing box model containing variables describing the skin thickness, spar thickness and stringer cross section separately tended to be the most reliable one for sizing. Hürlimann et al. [7] added representative pylon/engine and landing gear systems in the wing box model to allow the definition of engine and land gear loads. Dorbath et al. [16] further extended the structural modelling beyond the main wing box structure by including flaps and the wing-mounted flap tracks, allowing performing the sizing of flaps. Furthermore, to facilitate the load definition in FE models, Hürlimann et al. [26] compared the effects of load introduction methods on the sizing results. It was found that the switch from defining the aerodynamic loads using the high-fidelity nodal-based method to the low-fidelity SMT (i.e. shear, moment and torsion) method had negligible influence on the mass of the wing box. However, defining the fuel loads, engine loads and the loads for landing gear using the SMT method instead of the node-based method resulted in a 4% lighter wing. This difference is mainly attributed to the strengthening requirements caused by local stress concentration which cannot be specifically reflected when using the SMT methods.

1.4. Objectives of the present study

The up-to-date wing sizing methods and results that have been published vary significantly in terms of the applied design inputs (i.e. load cases, design constraints, modelling features, etc.). To the best of the authors' knowledge, there has been a lack of sufficient validations of the reported sizing results against real aircraft data, leading to uncertainties in the fidelity level of the reported sizing results. In addition, there have been few publications investigating the effects of different design inputs on the accuracy of preliminary sizing or summarising the key design inputs required by an accurate preliminary sizing of the wing box structure. Filling this gap would be beneficial for improving the accuracy and efficiency of preliminary sizing and mass estimation with simplified (but sufficient) design conditions, especially for research purposes.

In this paper, key design inputs for preliminary sizing based on a typical single-aisle civil aircraft wing are identified. Parametric wing box FE models describing the structural layout have been automatically generated and applied in this study, with typical load cases (representing flight manoeuvres, engine loads and landing & ground handling conditions) being defined in accordance with CS25 [37]. The

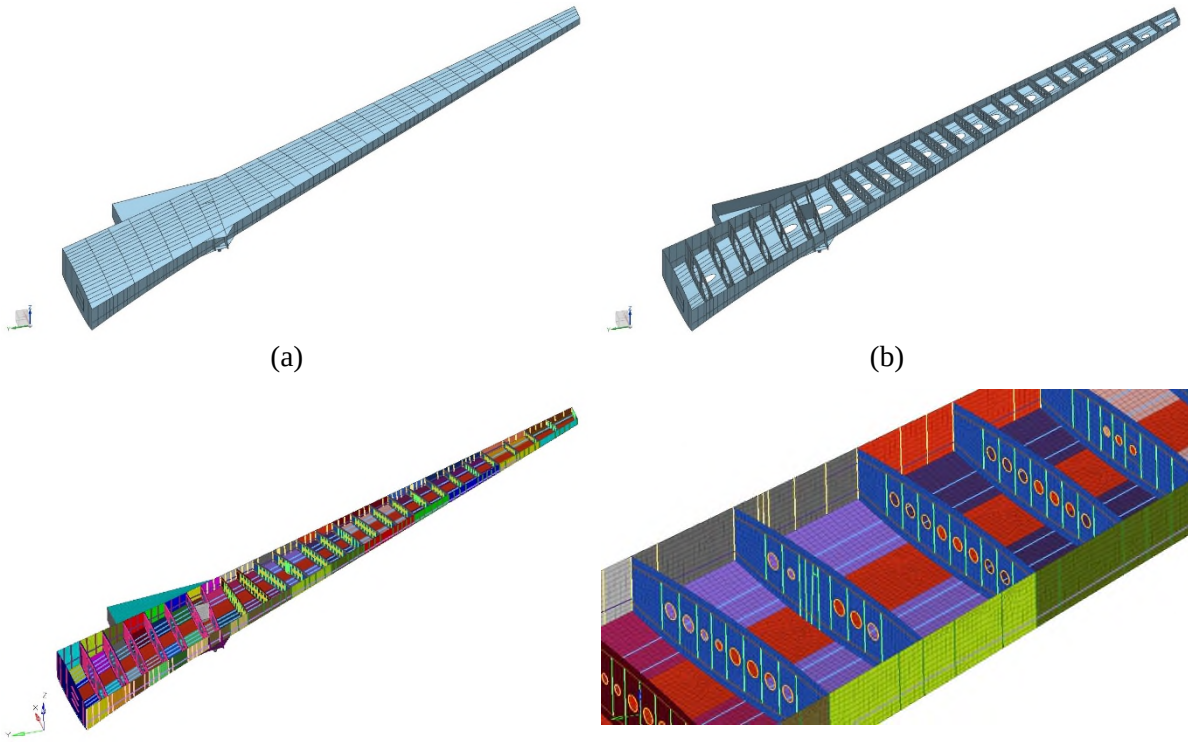
sizing process has been achieved using Nastran SOL200 based on gradient-based optimisation algorithms. The mass of the wing box resulting from sizing has been verified against a high-fidelity model, which was developed and validated based on a real wing box structure of the selected aircraft. A sensitivity analysis has been subsequently carried out to conclude the main factors affecting the accuracy of structural sizing and mass estimation. The influence of these factors on the static and modal behaviour of the sized wing structure has also been investigated.

2. Wing box models

2.1. High-fidelity baseline model

The high-fidelity wing box model (CAD), which is shown in Fig. 1 (a) and Fig. 1 (b), was reconstructed based on a real wing box, which is located at the Aerospace Integration Research Centre (AIRC) of Cranfield University. It was dissembled from an ex-service aircraft belonging to a type of classical single-aisle civil airliner, with its maximum take-off weight (MTOW) and wing span being around 78 t and 34 m respectively. Detailed information including the overall dimensions, the structural layout and local dimensions (e.g. panel thickness and stringer cross sections) of the selected wing box was obtained by manual measurements on the real structure and was reflected in the high-fidelity model. In addition to the key components such as top and bottom skins, front and rear spars and ribs, this model contains structural details such as cutouts on ribs, stiffeners on ribs and spars, and stringers attached on the skins, but excludes the secondary structures such as the leading edge (LE) and trailing edge (TE). An FE model was generated by meshing the CAD model using 75950 shell (i.e. CQUAD4) and 14983 beam (i.e. CBEAM) elements available in MSC Nastran (a de facto standard for the aerospace industry), considering the variation of panel thickness (for skins, spars and ribs) and stringer cross sections. The generated FE model is shown in Fig. 1 (c) with its zoom-in view within the wing box shown in Fig. 1 (d), where the lines on panels highlight the beam elements representing stiffeners or stringers. The connection between different components in the FE model was achieved by ensuring coincident nodes at the boundaries. The materials applied to each component and the associated properties are listed in Table 1.

Modal testing was carried out on the wing box structure at the AIRC, with the root of the wing box being constrained on the rig specifically designed for this test. The modal shapes and frequencies obtained from this test were used to validate the FE modal analysis results, which was obtained using the baseline wing box model with the root being constrained using RBE2 and CBUSH elements representing the test condition. The validation results are shown in Fig. 2. It can be seen that good match between test and FE analysis is obtained in terms of not only the modal frequencies, but also the modal shapes; modal assurance criterion (MAC) is a good statistic indicator and a degree of consistency between mode shapes (MAC = 1 represents completely consistent modal shapes). Therefore, it is reliable to apply this high-fidelity model as the baseline model in the present study for sizing validations.



(a) (b)

(c) (d)

Fig. 1. High-fidelity baseline wing box model: (a) the CAD model, (b) the internal structural layout, (c) the FE model and (d) its zoom-in view.

Table 1. Materials applied to each component of the wing box.

Component	**Material**	**E (GPa)**	**ν**	**ρ (g/cm^3)**	**σ_{yield} (MPa)**
Bottom skin/stringers	Al 2024-T351	73.1	0.33	2.78	330
Top skin/stringers	Al 7150-T651	71.7	0.33	2.83	570
Spars & ribs	Al 7010-T76	71.7	0.32	2.82	490

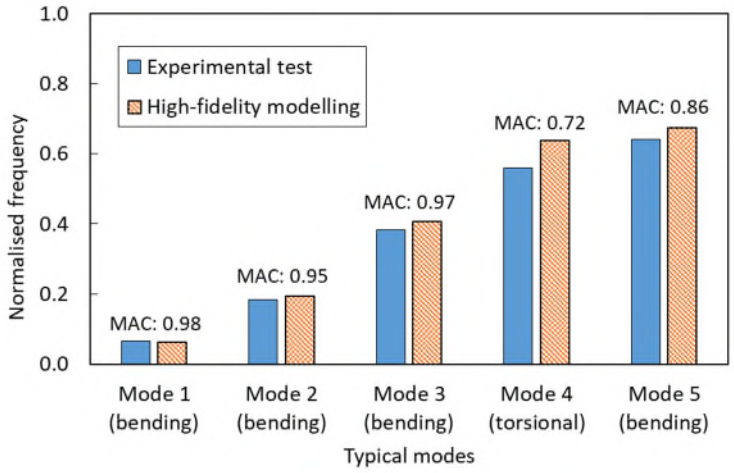


Fig. 2. Comparison between the modal responses obtained from modal testing on a real wing box structure and its high-fidelity FE model, in terms of modal frequency comparison and the modal assurance criterion (MAC).

2.2. Models used for sizing

The FE models used for preliminary sizing were generated by applying a TCL code developed for generating generic wing box models in Hypermesh, following the format of MSC Nastran input deck; TCL code is a coding language supported in Hypermesh, allowing a user to carry out modelling based on command lines. The configuration and structural layout of the investigated wing box were used as the input data of this code, being consistent with the high-fidelity baseline model shown in Fig. 1. It is noted that structural details such as cutouts and stiffeners on ribs and spars are excluded from this model, which are usually not considered until the detailed design stage. The same materials as the high-fidelity baseline model were applied to each component, as listed in Table 1.

The top skin, bottom skin, front spar and rear spar of the wing box model are divided into 13 sizing sections (one sizing section defined between every other ribs) to allow the spanwise variation of the panel thickness to be determined by the sizing process, as shown in Fig. 3(a). The ribs are also organised into 13 sizing groups in terms of their spanwise locations; ribs within the same group share a single panel thickness variable. The stringers attached on skins were modelled using CBEAM elements with their cross-section dimensions varying in the spanwise direction, based on actual measurements on the real wing. In order to reduce the complexity of sizing optimisation, the number of stringer distribution and their cross sectional spanwise variation were fixed to simplify the sizing process to only focus on panel thickness variations. In addition, the mass breakdown of the secondary structures was estimated using an empirical method introduced in [38], listed in Table 2. The mass distribution was then estimated based on the projected area of the secondary structures and was implemented in the FE model in terms of lumped masses distributed along the front and rear spars using CONM2 and RBE3 elements, as shown in Fig. 3(b).

To understand the effects of the number of sizing panels on the sizing results, a 26-section model, which allowed greater variation of panel thickness in the spanwise direction, was also generated, as illustrated in Fig. 3(c). In addition, a refined 26-section model shown in Fig. 3(d) was also generated by further refining the sizing patches in the chordwise direction, allowing chordwise skin thickness variance to be determined from sizing. The secondary structural mass listed in Table 2 were also added to these two models during the sizing process.

Table 2. Mass breakdown (in percentage) of the estimated secondary structure.

Weight chapter	Fixed leading edge	Fixed trailing edge	Leading-edge high-lift devices	Trailing-edge high-lift devices	Ailerons	Spoilers	Total
Mass (%)	17.4	10.7	20.0	41.4	3.4	7.1	100

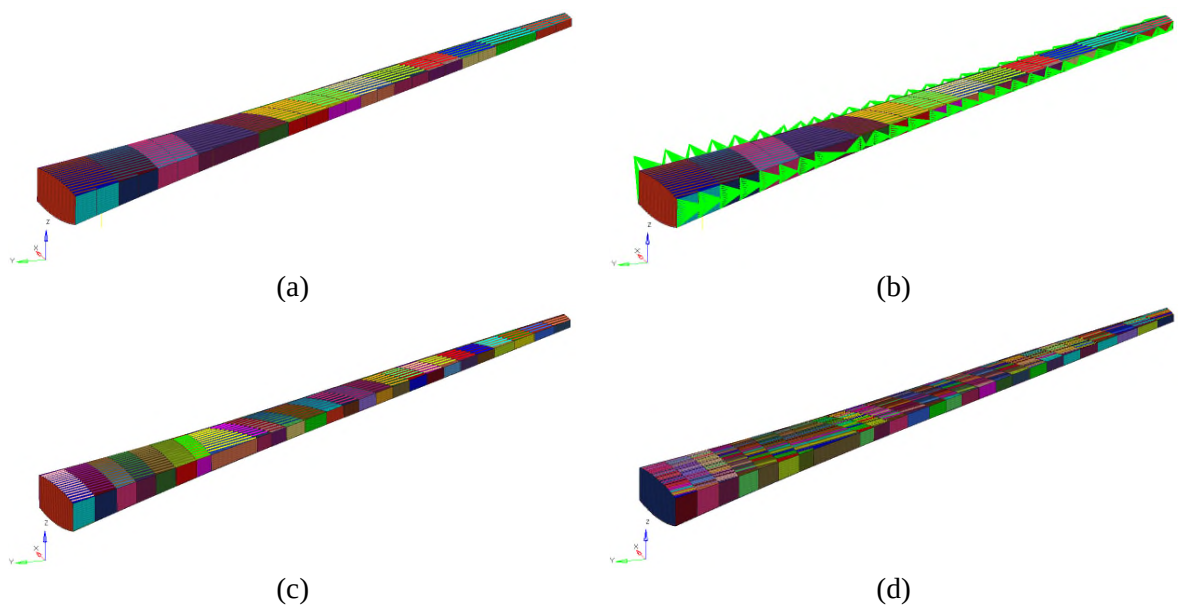


Fig. 3. (a) 13-section model, (b) 13-section model with lumped mass, (c) 26-section model and (d) refined 26-section model used for sizing of the wing box. The distribution of sizing panels is illustrated in terms of colour variance.

3. Sizing of the wing box

3.1. Load cases

In the design of a real aircraft, hundreds of load cases are considered to ensure each structural component is sufficiently strong to sustain the design loads. At the preliminary sizing stage, fewer load cases are required than detailed sizing since it mainly focuses on determining the internal load path/distribution between the main components, rather than performing precise sizing for details of each structure. Therefore, 11 load cases representing typical aircraft manoeuvres, engine loads, and landing and ground handling conditions were selected as the limit design loads for sizing in this study, listed in Table 3.

2.5g symmetric pull-up, -1.0g push-down, 2.0g flap down (by 40º) at landing and aircraft rolling (with ailerons deflected by 25º) have been selected as the typical aircraft manoeuvres used for wing box sizing. 1.0g cruise was also included in order to consider the fatigue criterion as introduced in Section 3.2. The aerodynamic loads associated with each aircraft manoeuvre were estimated using the vortex lattice method (VLM). It was developed based on the standard vortex lattice theory derived from the potential flow theory [39]; the wing is represented as a surface of discretised grids where the vortices are superimposed. It is noted that the aero-structural coupling effects were not considered in the load calculation applied in this study. To facilitate load introduction in the FE model, the obtained pressure distribution was converted into a list of lift forces and twist moments defined at 26 nodes (one node between every two adjacent ribs) distributed along the ¼ chord line [26]. Load transfer from the loading nodes to the structure is achieved using the RBE3 element, as illustrated in Fig. 4. It is noted that although the structure of the LE, flaps and ailerons were not included in the FE model, the lift generated by them were calculated using VLM and was equivalently distributed to the wing box using the above method. In addition, inertial effects resulting from the mass of the wing box and secondary structures were also applied in the model together with each aircraft manoeuvre load case.

Table 3. Load cases applied for wing box sizing.

ID	**Load type**	**Description**	**Details**
1	Aircraft manoeuvre (aerodynamic) loads	Symmetric pull-up	2.5g symmetric pull-up, VD
2		Cruise	1.0g symmetric, VC
3		Symmetric push-down	-1.0g symmetric, VC
4		Flap down at landing	2.0g flap down 40 degrees, VFE
5		Aircraft rolling	Aileron +/- 25 degrees, VD
6	Engine loads	Engine max load at cruise	6.5g vertical + 1.5*max cruise thrust
			-3.5g vertical + 1.0*max cruise thrust
7		Engine max load at take-off	3.0g vertical + 3.0*max take-off thrust
			3.0g vertical + 3.0*reverse thrust
8		Engine max side loads	+/- 3.0g side
9	Landing and ground handling loads	Critical level landing condition	0.75 peak GRFz (vertical) + 0.3 V peak GRFz (drag) + 0.1875 peak GRFz (side)
10		Critical side load condition (lateral drift)	0.5 peak GRFz (vertical) + 0.4 peak GRFz (side)
11		Braked roll condition	0.6 peak GRFz (vertical) + 0.48 peak GRFz (drag)

* VD: design dive speed; VC: design cruise speed; VFE: maximum flap-extended speed; GRFz: maximum vertical ground reaction force.

To investigate the effects of engine loads on wing box sizing, three load cases representing the critical thrust and inertial loading conditions of the engine were selected [40]. CFM56-5B7 was selected as the reference engine and its thrust specifications were used to calculate the engine loads applied in sizing; the max take-off and cruise thrust of CFM56-5B7 is 120 kN and 26 kN respectively. In the FE model, the engine loads were defined at the engine CG (i.e. centre of gravity), where a point mass of 3,751 kg was also defined to represent the mass of the engine. To accurately transfer the engine loads into the wing box structure, a truss-based pylon/engine representation structure shown in Fig. 5 was created in the model using CBEAM elements, with the pylon-wing connection fittings defined using RBE3 elements. To ensure a determinate mounting system, the front fittings take vertical (z) loads only, the thrust link takes thrust (x) and side (y) loads, and the rear fitting takes vertical (z) and side (y) loads.

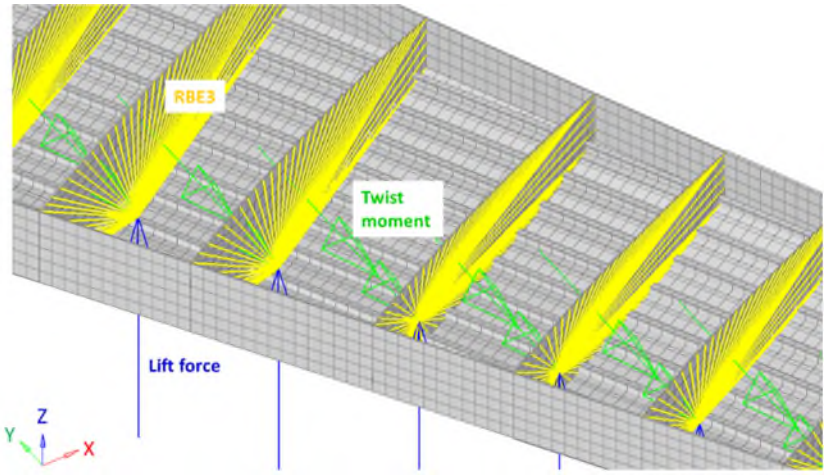


Fig. 4. Illustration of the application of aerodynamic loads to the wing box (with top skin being hided).

Critical landing and ground handling loads were also included in the sizing load cases. The selected load cases include the critical level landing, lateral drift and braked roll conditions with corresponding load factors defined according to CS-25 [37]. The maximum vertical ground reaction force (peak GRFz) designed for the landing of the investigated single-aisle civil aircraft is estimated to be 1.2 MLW (maximum landing weight: 64,450 kg) [40]. In the FE model, a truss-based structure (using CBEAM elements) representing the landing gear system was created to ensure that the defined landing loads were appropriately transferred to the wing box structure, as shown in Fig. 6; the connection between the landing gear system and the wing box structure was defined using RBE3 elements.

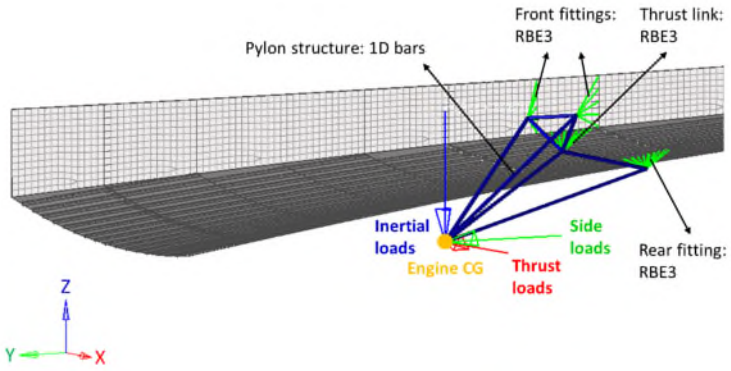


Fig. 5. Pylon and engine representation with typical engine loads.

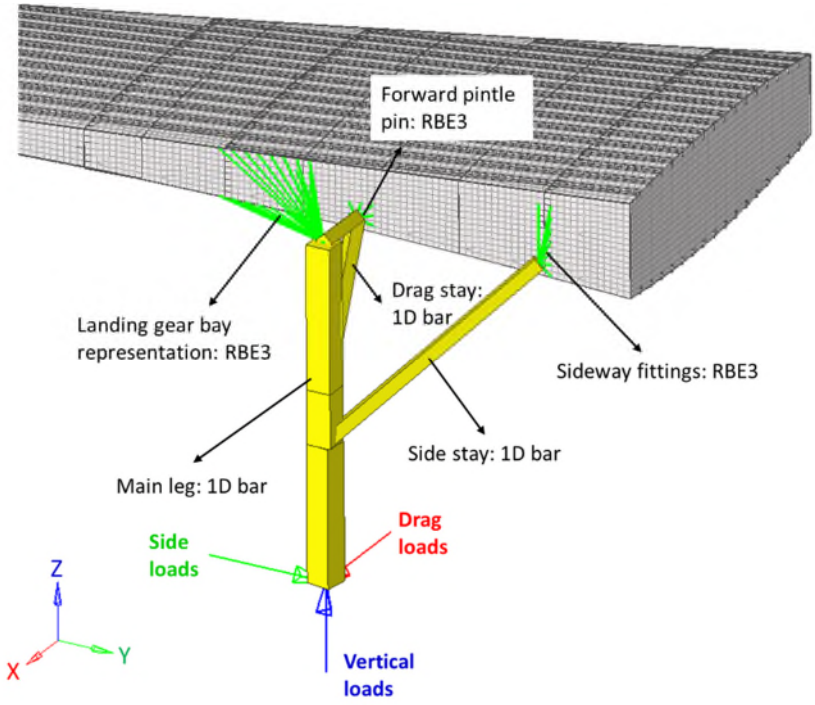


Fig. 6. Landing gear system representation with typical landing loads.

3.2. Structural sizing criteria

The sizing process was realised using Nastran SOL200 based on a gradient-based optimisation algorithm, aiming at minimising the structural mass. The objective, design variables and constraints of the optimisation were defined in the Nastran input file. The design variables refer to the thickness value of the panel for each section of the wing box component; the thickness value can be adjusted to meet the target of minimum mass while ensuring that all the constraint conditions are satisfied. The 13-section wing box model contains 13 design variables for each component (i.e. top skin, bottom skin, front spar, rear spar and ribs) and hence 65 variables in total. By contrast, the 26-section and the refined 26-section models contain 130 and 590 design variables respectively.

Both strength and buckling criteria were used as design constraints of sizing for each component. The strength criterion required the von Mises stress not exceeding σ_{yield} at the limit load with a reserve

factor of 1.0. This criterion was satisfied by monitoring the peak stress value within each sizing panel. The buckling criterion required the structure to be free from buckling at the limit load with a reserve factor of 1.0. This was realised by constraining the first 20 buckling modes obtained from the FE analysis; the eigenvalue λ for each mode was constrained to be not lower than 1.0. It's noted that the effects of imperfections on buckling response of the whole wing box were not considered at this stage, but should be incorporated into the part model at the stage of detailed design. In addition, fatigue criterion was also applied for the bottom skin design. The 1.0g cruise load case multiplied by a factor of 1.3 was chosen as the fatigue design loads to account for gust effects during flight [27]. A critical fatigue stress value of 100 N/mm^2 was used in the applied fatigue criterion. This value is lower than the fatigue resistance of Al 2024-T351 (i.e. 138 N/mm^2) and was regarded as a reasonable value during aircraft preliminary design due to the imperfections in the structure (e.g. manholes or rivets) [27].

3.3. Sizing results

Structural sizing was carried out using the 13-section, 26-section and refined 26-section models (as shown in Fig. 3) respectively based on the defined load cases and sizing criteria mentioned above. The sizing results for skins, spars and ribs obtained from each model are compared in Fig. 7 in terms of the spanwise (from wing root to the tip) thickness distribution for each component. Fig. 7 shows that similar trends of thickness distribution can be obtained using models with different discretised sections, particularly the 'peaks' representing local strengthening required by the attached landing gear system, pylon & engine structures and aircraft rolling loads. Fig. 7 also displays that the variation of local thickness distribution becomes greater when the applied number of design fields increases. In addition, compared to the 13- and 26-section models, chordwise skin thickness variation can be captured by the refined 26-section model, as shown in Fig. 7(a) and (b): front, middle and rear in the legend represent the chordwise location on the skin, as illustrated in Fig. 7(f). This difference in skin thickness distribution resulting from sizing using the three models are further illustrated by the contour plots shown in Fig. 8.

It is also noteworthy that the thickness distribution on real aircraft wings are a result of a more complicated detailed sizing process, where a higher fidelity analysis is implemented with more accurate load cases and models than preliminary sizing stage. Considering that the purpose of this study is to identify the key inputs affecting the preliminary sizing results rather than carrying out detailed sizing meeting the flight requirements, the sizing results displayed in Fig. 7 and Fig. 8 are deemed acceptable as long as the main effects of the typical loads are captured.

In addition to the thickness of each structural component, the mass of the resultant wing after sizing was also calculated from the FE model. The total mass of the sized wing box models obtained in the present study are compared to the high-fidelity baseline model, as listed in Table 4. It shows that by increasing the number of design fields from the 13-section to the refined 26-section model, the mass

difference between the sized and the baseline models is reduced. The case with the most design fields (i.e. the refined 26-section sizing) yields the best match with the baseline model; the estimated mass is 0.8% lower than the mass of the baseline model. However, it can be also expected that further refined sizing sections (with more design fields) may lead to underestimation of the wing structural mass.

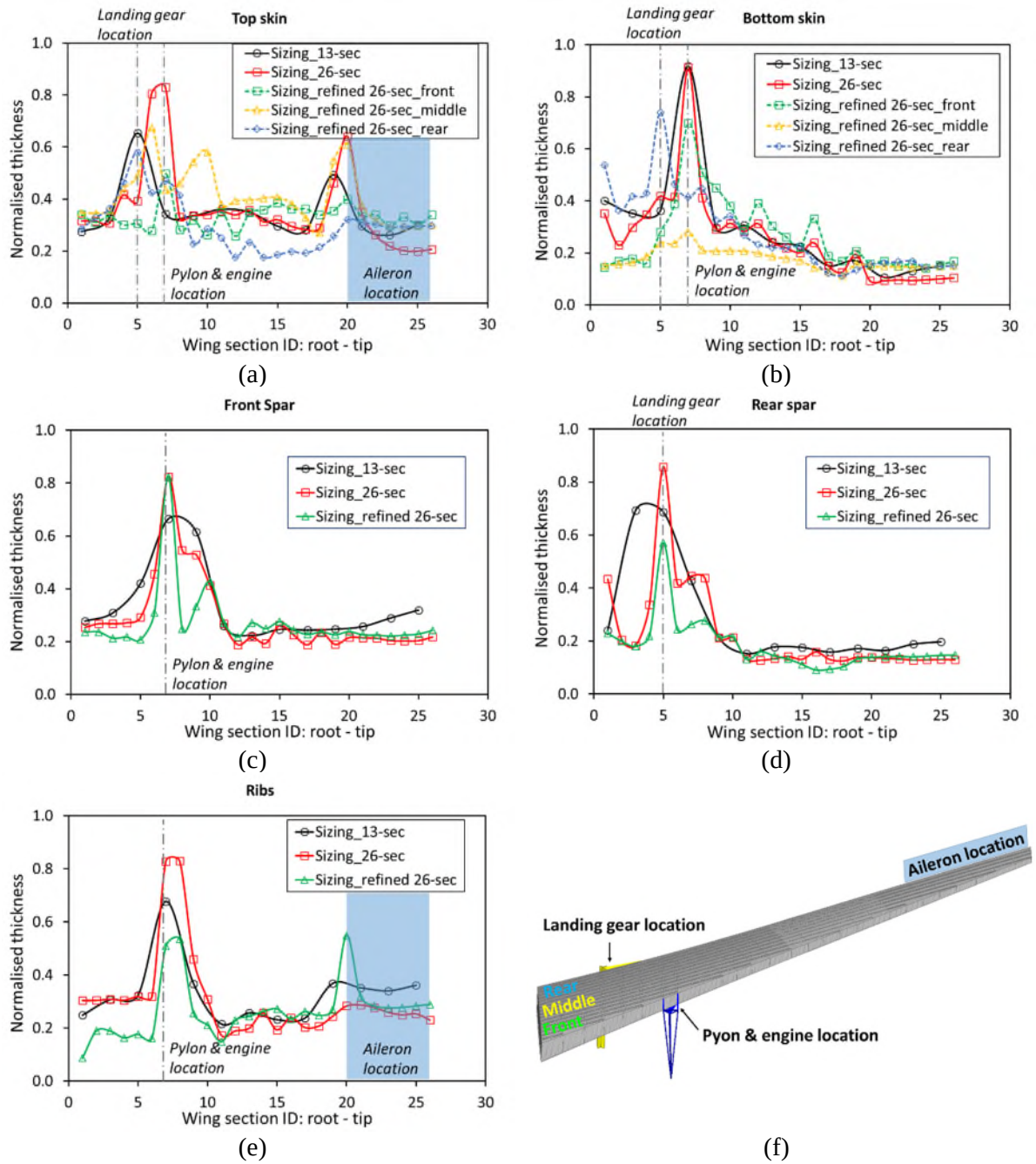


Fig. 7. Comparison between the sizing results obtained using the 13-section, 26-section and refined 26-section models: (a) top skin, (b) bottom skin, (c) front spar, (d) rear spar and (e) ribs. (f) Illustration of the locations of landing gear, pylon & engine and aileron relative to the wing box.

The mass breakdown of the corresponding wing box structure is shown in Fig. 9, comparing the mass of each structural component obtained from the high-fidelity baseline and sized models, excluding the mass of secondary structures. Similar trend with the comparison in total mass (Table 4) can be seen for

most components when the number of design fields is increased, particularly for the bottom skin/stringers. This trend is due to the fact that a real wing design always requires reasonable thickness variation to allow effective weight saving design. Limited number of design fields, however, may have insufficient sizing flexibility to support the required thickness variation, hence tends to overestimate the mass. By contrast, excessively number of design fields may lead to significant or irregular thickness variance between adjacent sizing panels, making the associated manufacturing less practical. This, inversely, tends to underestimate the mass of the manufacturable wing in reality. Therefore, appropriate choice of the number of design fields is critical for an accurate mass estimation of the wing at the preliminary design stage.

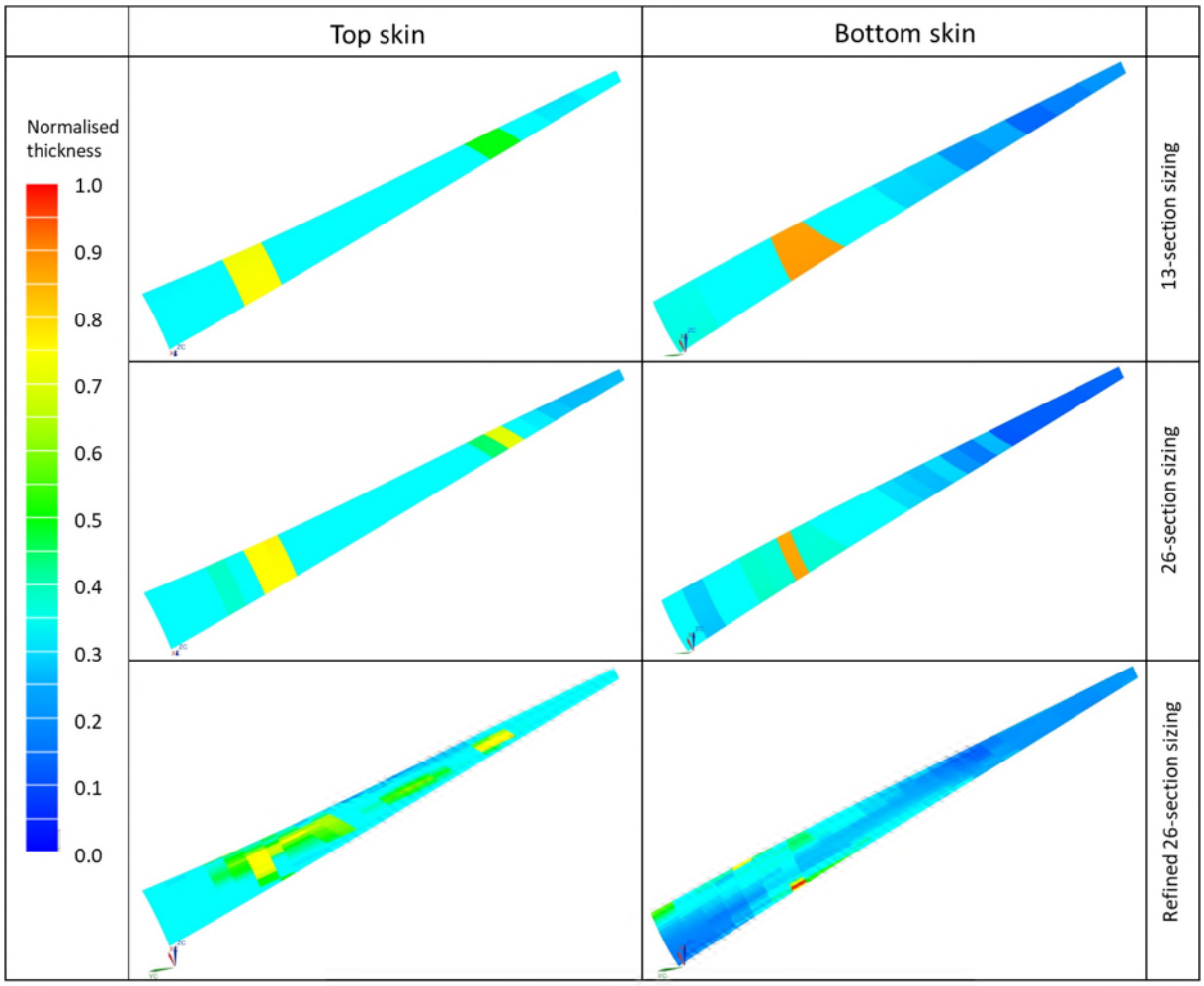


Fig. 8. Skin thickness distribution obtained from sizing using the 13-section, 26-section and refined 26-section models.

Table 4. Mass difference between the wing box models obtained from sizing and the high-fidelity baseline model (excluding the mass of secondary structures).

	13-section model	26-section model	Refined 26-section model
Mass difference (compared to the baseline model)	23.4%	15.2%	-0.8%

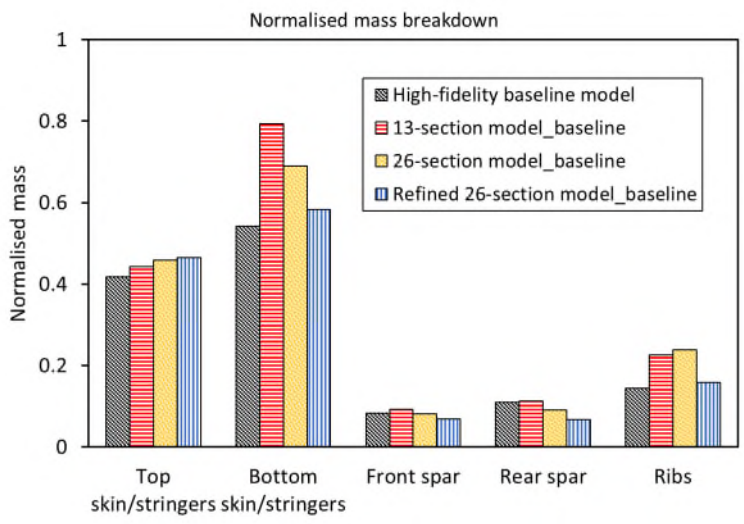
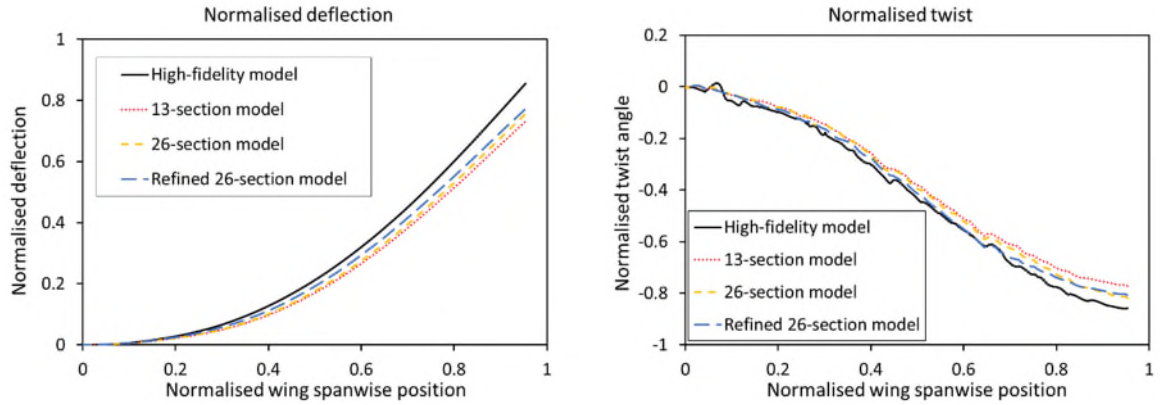


Fig. 9. Mass breakdown of the investigated wing box structure obtained from the high-fidelity baseline and sized models.

3.4. Structural behaviour of the designed wing box

The static and modal behaviours of the wing box models obtained from sizing were compared to the high-fidelity baseline model. The purpose of this comparison is to investigate the effects of the accuracy of sizing and mass estimation on the structural behaviour of the sized wing. The deflection and twist angle profiles along the wing span under 2.5g static loads are displayed in Fig. 10. It can be seen that the sized wing box models demonstrate similar static behaviour as the baseline model with the greatest difference occurring at the wing tip. The comparison between the tip displacement and twist angle of the sized and baseline models are listed in Table 5. It shows that the refined 26-section model generates the most consistent static behaviour with the baseline model, with the difference in tip deflection and twist angle being -10.9% and -5.9% respectively. By contrast, the 13-section and 26-section models lead to greater difference (-11% to -24%), which is due to the overestimation of the wing box structure stiffness by the sizing process.

Similar comparison has also been carried out for the modal behaviour. The comparison between the 1st bending, 2nd bending and 1st torsional modal frequencies of the sized and baseline models are listed in Table 6. The sized models demonstrate good match (i.e. difference < 5%) with the baseline model regardless of the number of design fields, except the 1st torsional mode obtained from the 13-section sizing. Generally, the comparison in modal frequencies presented in Table 6 shows better consistency than that in mass and static behaviour (stiffness), which is due to that the effects of the overestimated mass and stiffness tend to be counteracted.



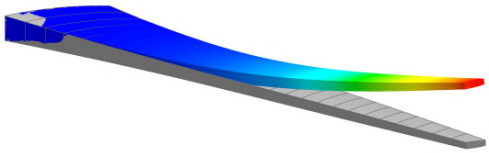
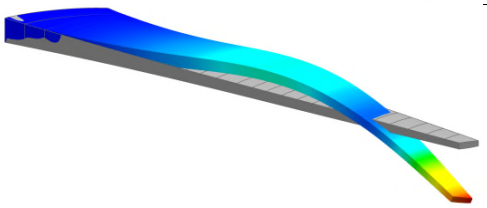
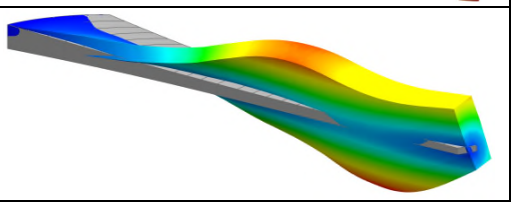
(a) (b)

Fig. 10. Comparison in the static wing behaviour (under 2.5g symmetric loads) between the sized and the high-fidelity baseline wing box models: (a) deflection and (b) twist angle.

Table 5. Comparison of the static behaviour (deflection and twist angle at wing tip) between the sized and the high-fidelity baseline wing box models.

	13-section model	26-section model	Refined 26-section model
Difference in deflection at wing tip	-23.2%	-15.8%	-10.9%
Difference in twist angle at wing tip	-19.5%	-11.4%	-5.9%

Table 6. Comparison of the modal behaviour between the sized and the high-fidelity baseline wing box models.

		13-section model	26-section model	Refined 26-section model	Modal shape
Difference in modal frequency	1st bending mode	-3.6%	-1.5%	2.3%	
	2nd bending mode	2.5%	2.9%	4.4%	
	1st torsional mode	-6.2%	-0.6%	-0.3%	

4. Results and discussions

Section 3 demonstrates that sensible sizing and mass estimation results can be obtained for preliminary design of the wing by applying the strength, buckling and fatigue constraints with the design load cases listed in Table 3. Understanding the role of these load cases and constraints in sizing and mass estimation would be helpful to identify the key design inputs that are essential for an accurate and efficient sizing process of the wing box structure. To achieve this, a sensitivity analysis on the effects of the applied loads/constraints on the mass and structural behaviour of the designed wing was carried out. As shown in Table 7, this analysis comprises of 10 steps. The simplest case, also the most commonly applied design inputs (i.e. 2.5g symmetric pull-up loads + strength constraint), is applied in Step 1. In subsequent steps, the complexity of the applied design inputs is gradually increased by adding more load cases or design constraints. The sequence of loads/constraints may produce different sensitivity outputs, therefore careful selection of these sequence was made based on two principles:

a. Add the common or frequent applied loads/constraints (according to references and general practice) prior to those less frequently adopted in wing box design.
b. Place global loads/constraints earlier in the sequence relative to local ones.

This came up with the applied design inputs for each step of the sensitivity analysis, as shown in Table 7. The buckling constraint, as the most commonly applied global design constraint in addition to strength, was introduced in Step 2. Another two frequently applied global design inputs, the inertial force resulting from the wing box and secondary structures (i.e. LE & TE), were introduced in Step 3 and 4 respectively. The fatigue constraint was then added in Step 5, which mainly affected the sizing of the bottom skin. In addition, the effects of specific aircraft manoeuvre loads (i.e. push-down, flap down and aircraft rolling) were included from Step 6 onwards. With 2.5g loads being considered, the influence of these load cases on sizing tend to be localised. Finally, more local load cases, critical engine loads and landing & ground handling loads, were taken into account in Step 9 and 10 respectively. Both the 13-section and 26-section wing box models were applied in this sensitivity analysis; the refined 26-section model was not applied due to its low computing efficiency for this analysis. It is noteworthy that the models used in Step 10 correspond to the ones applied in Section 3.

Table 7. The design load cases and constraints (i.e. sizing inputs) applied in each step of the sensitivity analysis.

Step	**Load cases ID and description**	**Design constraints**
1	1 (2.5g symmetric pull-up, no inertial loads)	Strength
2	1 (2.5g symmetric pull-up, no inertial loads)	Strength and buckling
3	1 (2.5g symmetric pull-up, wing box inertial loads added)	Strength and buckling
4	1 (2.5g symmetric pull-up, wing box and LE & TE inertial loads added)	Strength and buckling

5	1 – 2 (1.0g symmetric loads and fatigue constraint added)	Strength, buckling and fatigue
6	1 – 3 (-1.0g symmetric loads added)	Strength, buckling and fatigue
7	1 – 4 (2.0g flap down loads added)	Strength, buckling and fatigue
8	1 – 5 (aircraft rolling loads added)	Strength, buckling and fatigue
9	1 – 8 (critical engine loads added)	Strength, buckling and fatigue
10	1 – 11 (landing & ground handling loads added)	Strength, buckling and fatigue

* The ID of the load cases refers to Table 3.

It is noted that although neglecting the aero-structural coupling effects tends to affect the accuracy of aerodynamic load calculation, the sensitivity analysis based on Table 7 is still expected to provide useful information on the relative importance of the listed design loads and constraints, particularly for those local concentrated design loads (i.e. engine loads, landing loads, etc.), which hardly depends on the aero-structural coupling effects.

4.1. The effects of the design inputs applied in sizing on mass estimation

The masses of the sized wing box structure resulting from each step of the sensitivity analysis are summarised in Fig. 11. The presented mass change is defined by Eq.1, where ΔM represents the increased/decreased mass between adjacent steps by updating the design inputs of sizing according to Table 7, M_B is the total mass of the high-fidelity baseline model. Greater mass change indicates higher importance of considering the added sizing input in improving the accuracy of mass estimation. Eq.1 can also be used to similar analysis for static and modal behaviour of the wing by replacing the mass value in Eq.1 with deflection (or twist angle) and modal frequency respectively, which will be applied in Section 4.2.

$$\text{Mass change } (\%) = \frac{\Delta M}{M_B} \times 100 \tag{1}$$

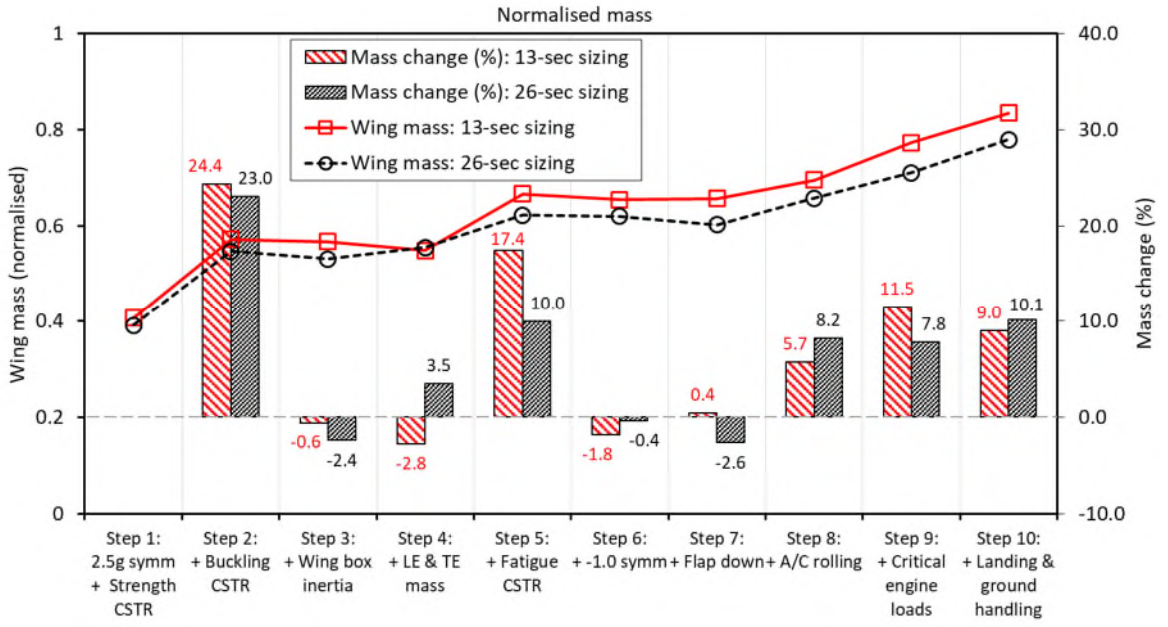
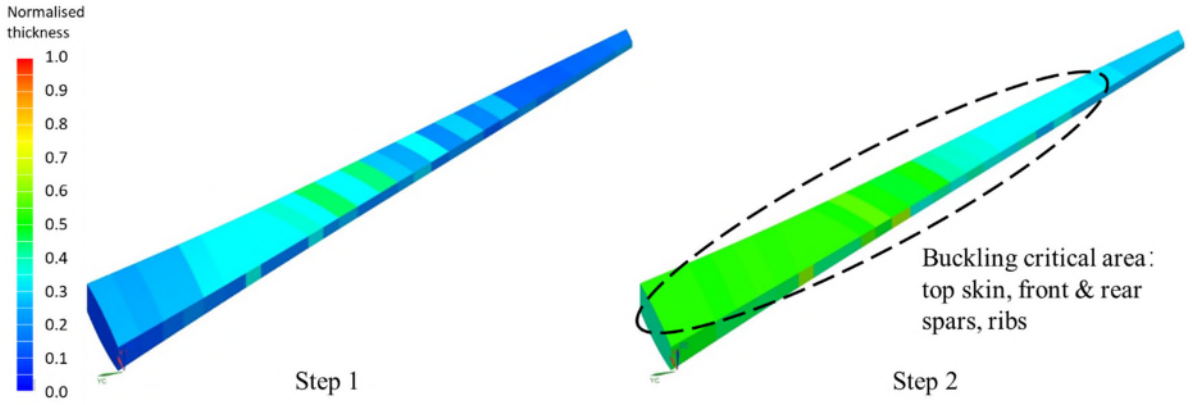


Fig. 11. The mass of the wing box structure obtained at each step of the sensitivity analysis using the 13- and 26-section models, together with the mass change by enriching the sizing inputs in each step.

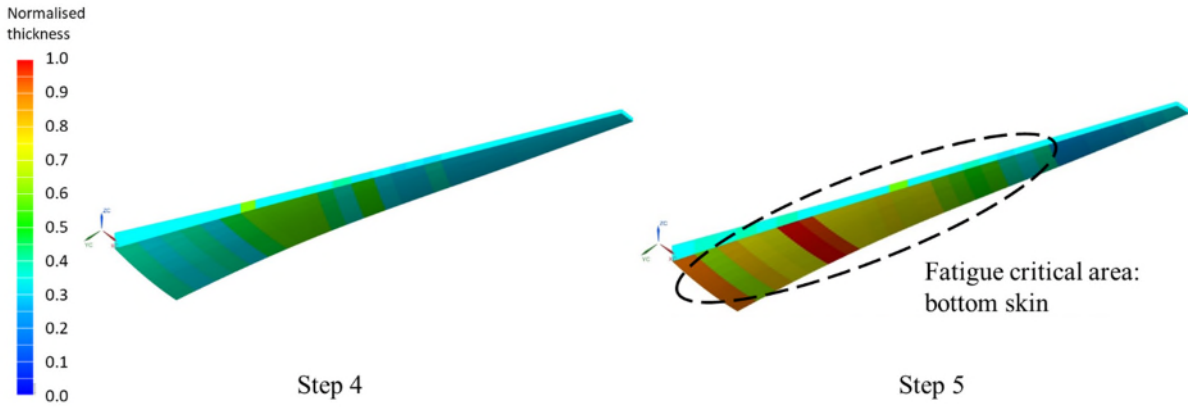
According to Fig. 11, similar trends can be obtained by applying the 13- and 26-section sizing. For brevity, the following discussion is based on the 26-section sizing results unless stated otherwise. It can be seen that simply applying the 2.5g symmetric loads and the strength constraint in Step 1 results in a wing box mass of ~0.4 (normalised value), implying a ~50% underestimation compared to the mass obtained in Step 10. The estimated mass gradually increases by enriching the designed load cases/constraints from Step 1 to 10.

According to Fig. 11, the buckling and fatigue constraints, the aircraft rolling loads, the engine loads and the landing & ground handling loads are regarded as the five inputs that most significantly affect the mass of the sized wing box, with a resultant mass increase of 23.0%, 10.0%, 8.2%, 7.8% and 10.1% respectively. The mass increase is attributed to the local strengthening requirements when these inputs are considered in sizing, which are illustrated in Fig. 12 by comparing the panel thickness distribution resulting from different steps of the sensitivity analysis.

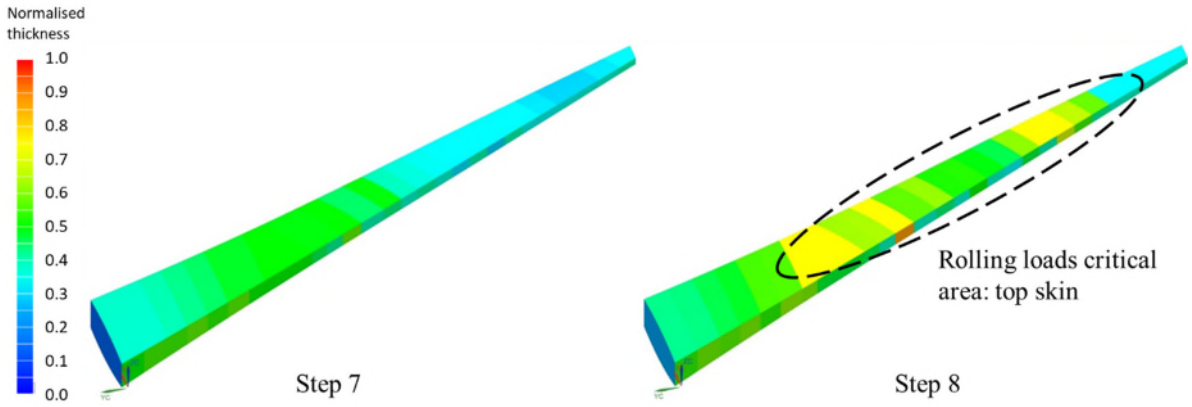
By contrast, the inertial forces arising from both the wing box and the secondary structural masses, the -1.0g push-down loads and the 2.0g flap down loads have relatively small effects (< 5%) on the overall mass of the designed wing box structure. It is noted that the reported mass change values caused by introducing these small-influencing features have limited practical meaning since they are predominantly affected by the numerical errors of sizing calculation rather than the design conditions.


Normalised thickness
1.0
0.9
0.8
0.7
0.6
0.5
0.4
0.3
0.2
0.1
0.0
Step 1
Buckling critical area: top skin, front & rear spars, ribs
Step 2

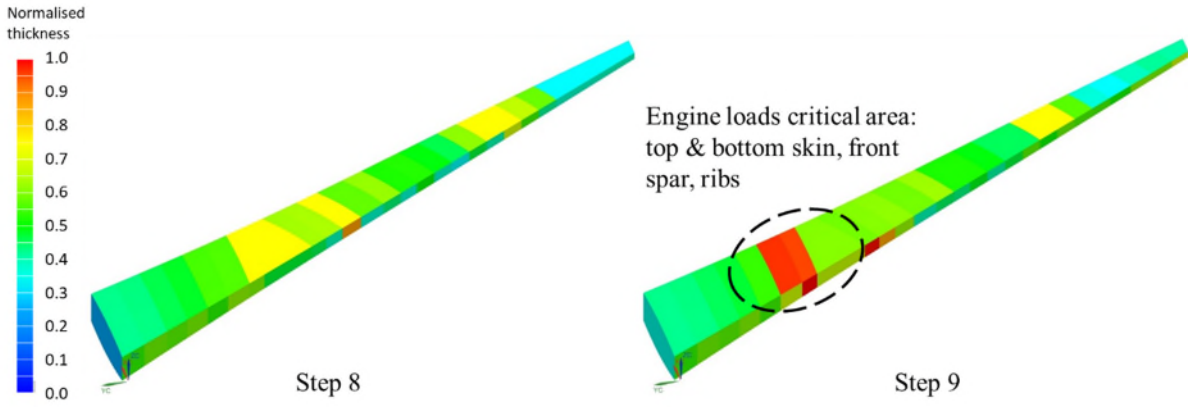
(a)


Normalised thickness
1.0
0.9
0.8
0.7
0.6
0.5
0.4
0.3
0.2
0.1
0.0
Step 4
Fatigue critical area: bottom skin
Step 5

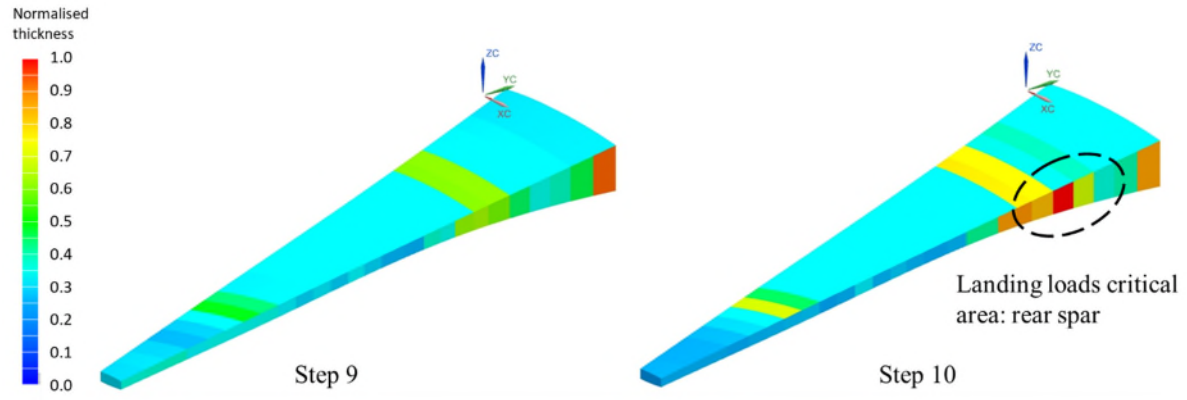
(b)


Normalised thickness
1.0
0.9
0.8
0.7
0.6
0.5
0.4
0.3
0.2
0.1
0.0
Step 7
Rolling loads critical area: top skin
Step 8

(c)


Normalised thickness
1.0
0.9
0.8
0.7
0.6
0.5
0.4
0.3
0.2
0.1
0.0
Step 8
Engine loads critical area: top & bottom skin, front spar, ribs
Step 9

(d)



(e)

Fig. 12. The effects of the considered design constraints/load cases in sizing (using the 26-section model) on panel thickness distribution: (a) buckling constraint by comparing Step 1 and 2; (b) fatigue constraint by comparing Step 4 and 5; (c) aircraft rolling loads by comparing Step 7 and 8; (d) engine loads by comparing Step 8 and 9; (c) landing & ground handling loads by comparing Step 9 and 10.

4.2. The effects of the design inputs applied in sizing on the structural behaviour of the designed wing

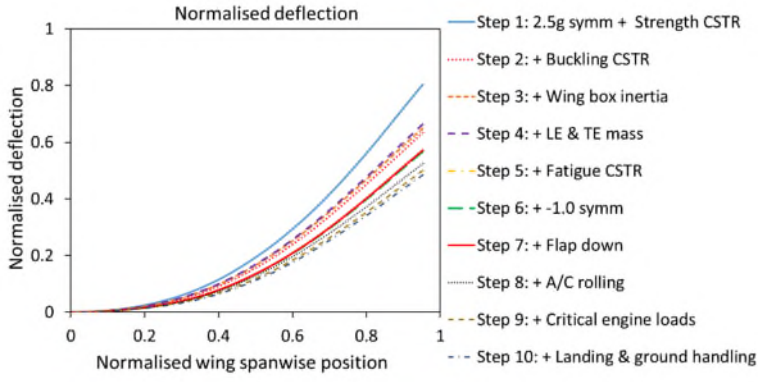
The structural behaviour of the sized wing box models resulting from each step of the sensitivity analysis listed in Table 7 were also investigated, using the 13- and 26-section models. The purpose is to figure out the design inputs (i.e. load cases and constraints) applied in sizing that are most critical to the overall structural performance of the designed wing; some design inputs might be necessary for localised structural design but may have negligible effects on the overall structural behaviour.

Similar to Section 3.4, 2.5g symmetric loads were applied to the models. The resultant deflection and twist angle of each model are illustrated in Fig. 13, demonstrating that the bending and torsional stiffness of the designed wing box structure increases (i.e. decreasing deflection and twist angle) when more design inputs are considered in sizing. To facilitate the comparison, the deflection and twist angle at the wing tip are summarised in Fig. 14, together with their changes in each step compared to the high-fidelity model; the definitions of these changes are similar with that for mass as expressed by Eq. 1. Similar with the mass analysis in Section 4.1, consistent trends are obtained from the 13- and 26-section sizing, hence for brevity, the following discussions are based on the 26-section sizing results unless stated otherwise.

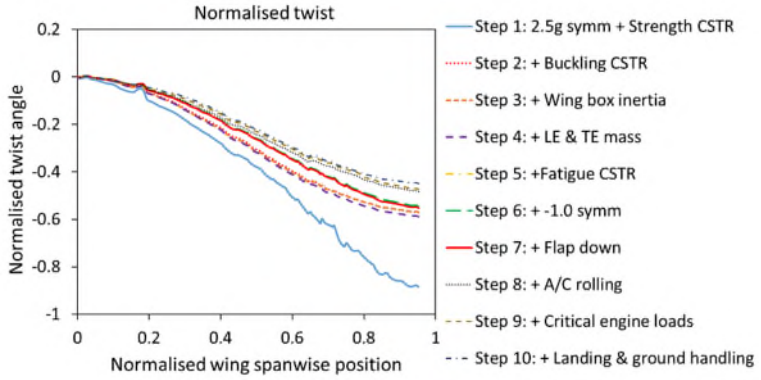
It can be seen that the most significant stiffness improvement of the designed wing arises from applying the buckling constraint in sizing: by 32.5% and 56.1% in bending and torsional stiffness respectively. Fig. 12(a) illustrates that it is attributed to the significant increase of the thickness of top skin and spars when the buckling constraint is considered in sizing. Another key design input is the fatigue constraint, which leads to a 14.8% (bending) and 10.7% (torsion) stiffer wing by strengthening the bottom skin panels (Fig. 12(b)). In addition, considering the aircraft rolling loads in sizing also improves the wing

box stiffness by 10.0% (bending) and 16.9% (torsion) via strengthening the top skin of the outboard wing ((Fig. 12(c)).

It is also noted that considering the critical engine loads and landing & ground handling conditions in sizing exert limited influence (< 5%) on the static performance of the sized wing box, being contrast to their influence on mass estimation. The reason accounting for this discrepancy is that the structural strengthening required by sustaining the engine and landing loads is localised (Fig. 12(d) and (e)), which has limited influence on the overall bending and torsional stiffness distribution of the wing box. In addition, considering the inertial forces, the -1.0g push-down and the 2.0g flap down loads are also deemed less critical for sizing a wing in terms of the static behaviour of the designed structure.

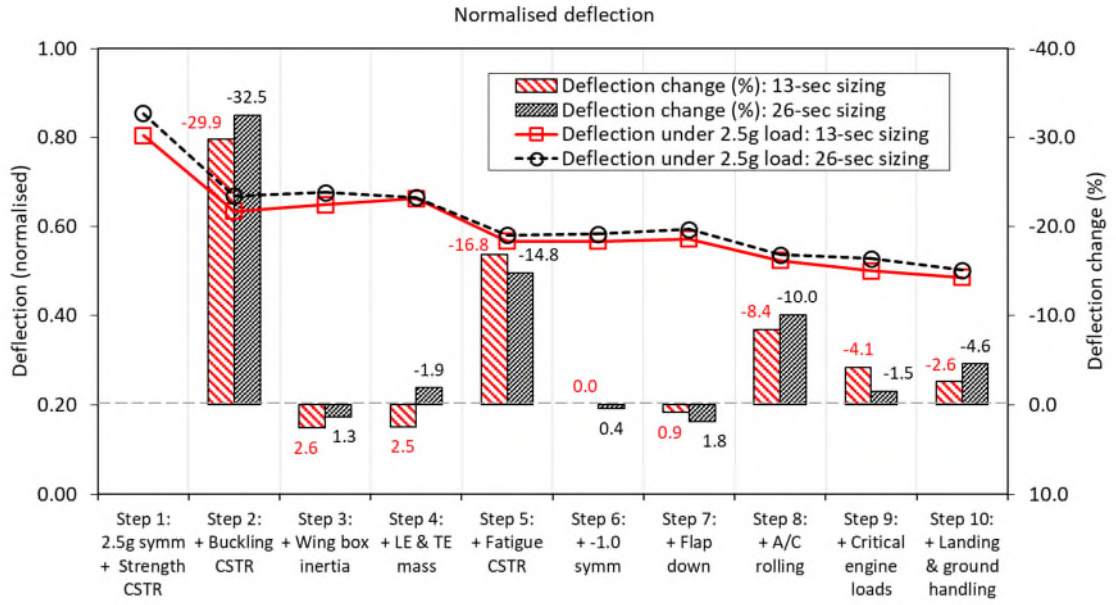


(a)

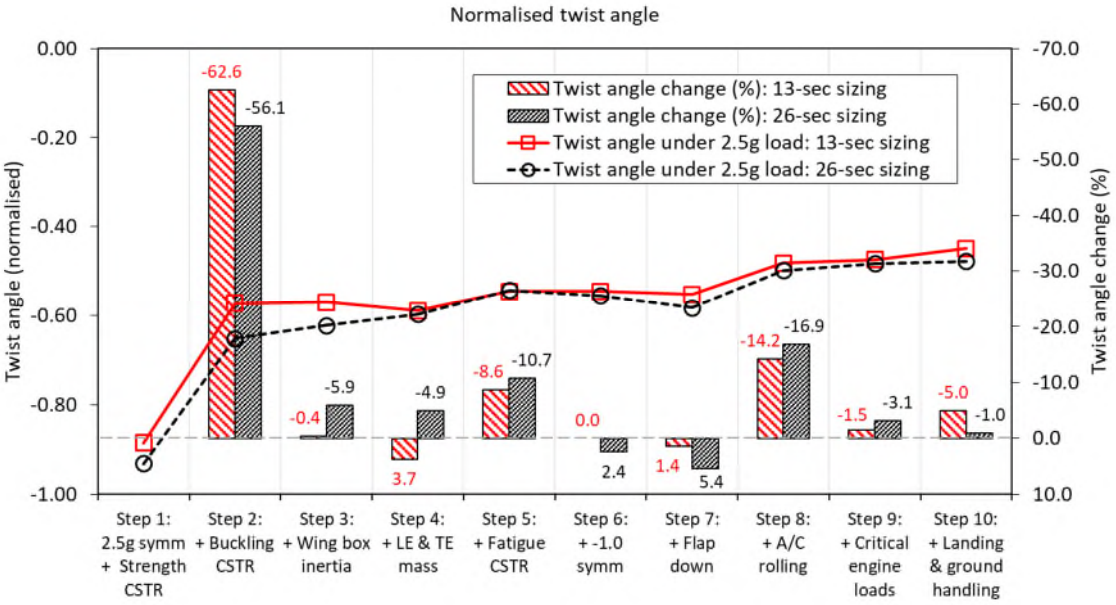


(b)

Fig. 13. (a) Deflection and (b) twist angle (under 2.5g static loading) of the designed wing box structure obtained at each step of the sensitivity analysis using the 26-section model.



(a)

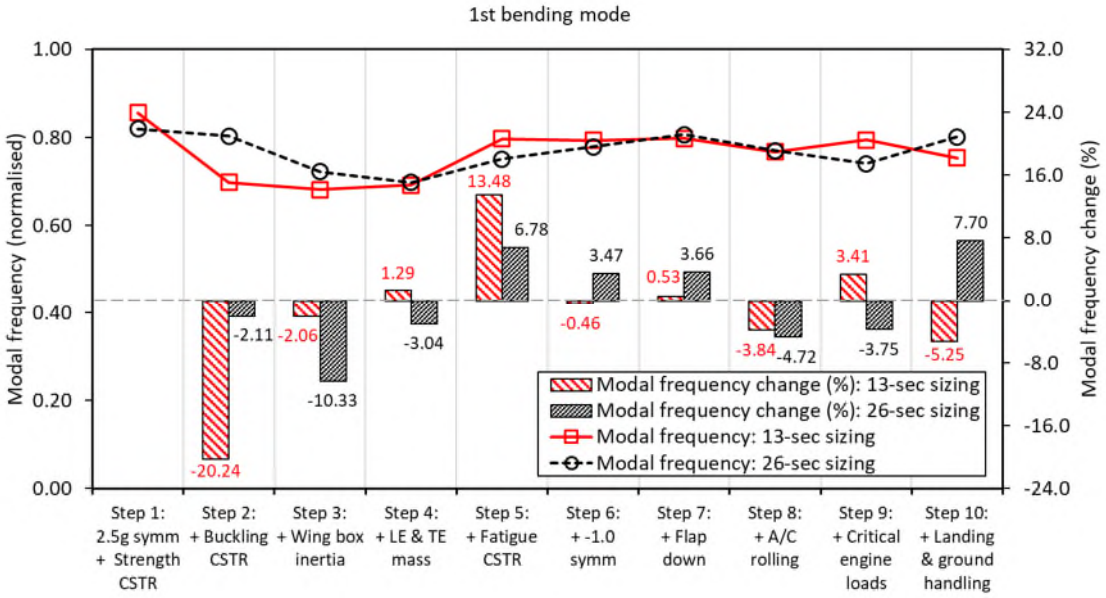


(b)

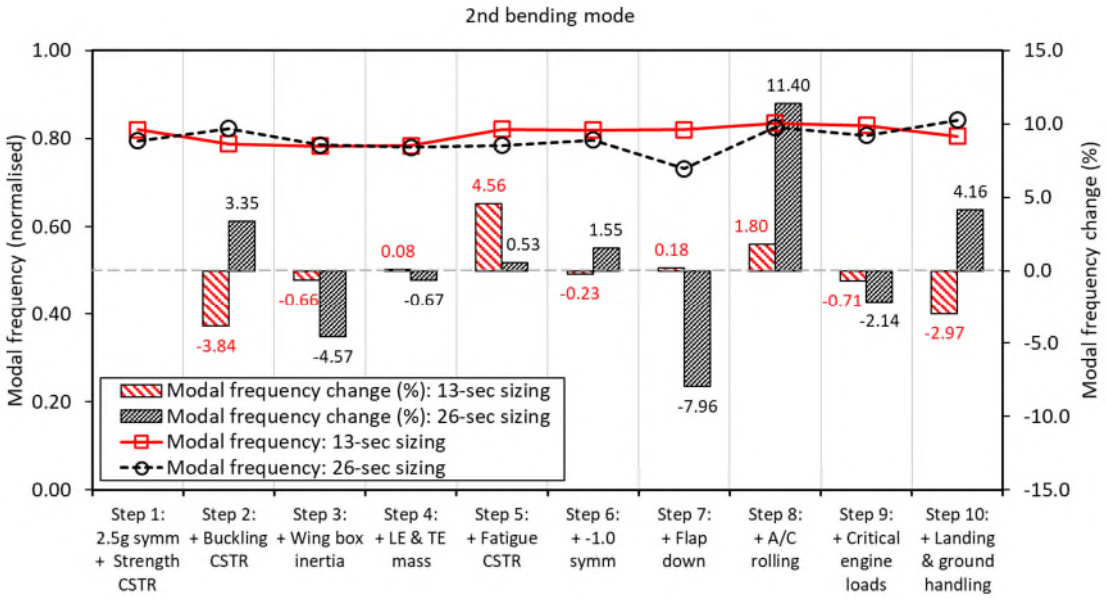
Fig. 14. (a) Deflection and (b) twist angle (under 2.5g static loading) at the tip of the wing box structure obtained at each step of the sensitivity analysis using the 13- and 26-section models, together with their changes by enriching the sizing inputs in each step.

In addition to the static performance, the sensitivity analysis was also implemented for the modal behaviour of the wing. Similar to Section 3.4, the 1st bending, 2nd bending and 1st torsional modes were chosen for this analysis. The corresponding modal frequencies of the wing box model obtained from each step of the sensitivity analysis using the 13- and 26-section models are illustrated in Fig. 15. The modal frequency changes in each step (compared to the high-fidelity baseline model) are also included in this figure, with similar definition as the mass change expressed by Eq. 1.

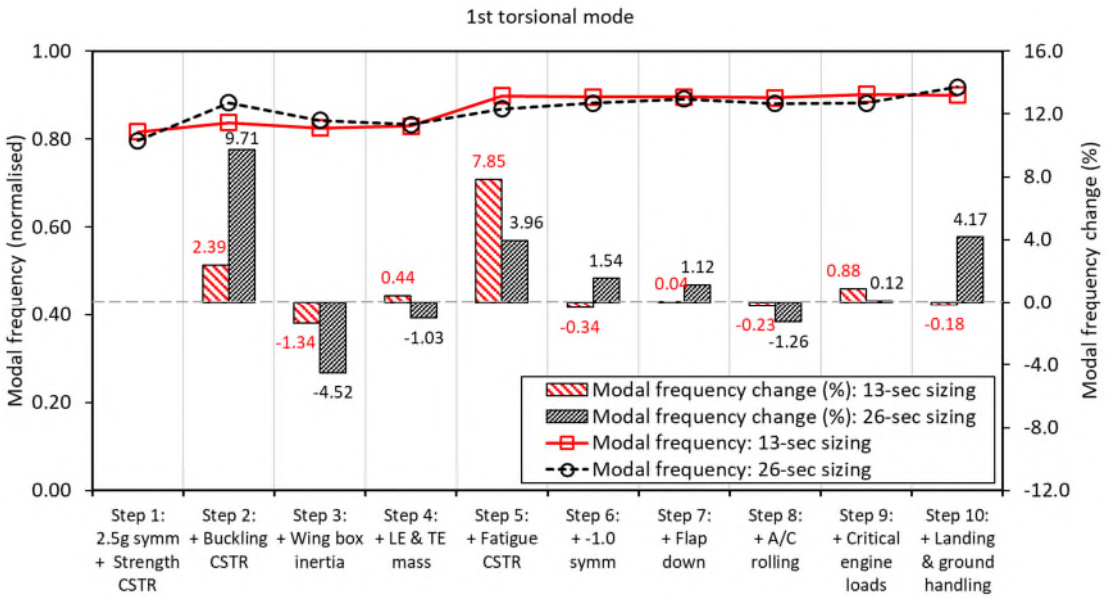
Being different with the mass and static (stiffness) analysis of the wing, the modal analysis demonstrates a fluctuated change in modal frequencies when the design inputs get enriched, as shown in Fig. 15; the modal frequency varies irregularly from Step 1 to 10, varying with modes. This less 'monotonic' trend is due to the competition between the mass and stiffness of the designed structure; the change in a specific modal frequency not only depends on the amount of the overall mass and stiffness changes, but also on their distributions. Therefore, a reliable way to obtain reasonable modal frequencies of the designed wing is to size it considering all the design inputs that are critical to both the mass (Fig. 11) and stiffness (Fig. 14) evaluation.



(a)



(b)



(c)

Fig. 15. Modal frequencies of the wing box structure obtained at each step of the sensitivity analysis, together with their changes by enriching the sizing inputs in each step: (a) 1st bending, (b) 2nd bending and (c) 1st torsional modes.

5. Conclusions

Preliminary sizing of the wing box structure of a single-aisle civil aircraft was successfully carried out using Nastran SOL200, based on a parametric wing box model. Some load cases including typical aircraft manoeuvres, engine loads, landing and ground handling conditions were considered as the load cases for sizing. The sizing results were verified against a validated high-fidelity wing box model which was developed based on the real wing.

The effects of the number of design fields were investigated by comparing the sizing results obtained using the 13-section, 26-section and refined 26-section wing box models. In this study, applying the refined 26-section model (with the most design fields) was found to result in the most accurate mass estimation and static behaviour compared to the real wing. However, it was also concluded that although more design fields allowed more flexibility of sizing in terms of the thickness variations within a component, it might result in an underestimation of the overall structural mass since the obtained thickness variation might be too restrictive to be manufactured.

A sensitivity analysis was also carried out to identify the critical design inputs (i.e. load cases and constraints) that are required to be considered for a reasonable preliminary design of a wing. It was found that in addition to the baseline design condition (i.e. 2.5g symmetric loads with strength constraint), the buckling and fatigue constraints, the aircraft rolling loads, the engine loads and landing & ground handling loads were the most critical design inputs for the overall mass of the sized wing, with a positive influence ranging between 7-24%.

Considering the buckling constraint, the fatigue constraint and aircraft rolling loads in sizing was also found to increase the stiffness (bending and torsional) of the designed wing by 32-57%, 10-15% and 10-17% respectively. The engine loads, landing and ground handling loads, by contrast, were deemed not as critical as their influence on mass estimation (within 5%), which is due to that the associated structural strengthening is mainly localised such that the overall stiffness of the wing is marginally affected.

In addition, it was also concluded that it was difficult to directly summarise the key design inputs for sizing that are critical to the modal behaviour of the designed wing. This is because that the modal frequency is largely dependent on the competition between the mass and stiffness distribution of the designed wing.

Acknowledgements

The authors would like to acknowledge Rolls-Royce plc for their support of this research as part of Powerplant Integration with Platform Systems (PIPS) Innovate UK project (UKRI113107).

References

[1] J. Dillinger, T. Klimmek, M.M. Abdalla, Z. Gürdal, Stiffness optimization of composite wings with aeroelastic constraints, J Aircraft 50(4) (2013) 1159-1168.

[2] S. Grihon, L. Krog, D. Bassir, Numerical optimization applied to structure sizing at AIRBUS: a multi-step process, International Journal for Simulation and Multidisciplinary Design Optimization 3(4) (2009) 432-442.

[3] G. Schuhmacher, I. Murra, L. Wang, A. Laxander, O. O'Leary, M. Herold, Multidisciplinary design optimization of a regional aircraft wing box, 9th AIAA/ISSMO Symposium on Multidisciplinary Analysis and Optimization, 2002, p. 5406.

[4] G. Bindolino, G. Ghiringhelli, S. Ricci, M. Terraneo, Multilevel Structural Optimization for Preliminary Wing-Box Weight Estimation, J Aircraft 47(2) (2010) 475-489.

[5] R. Ajaj, M. Friswell, D. Smith, A. Isikveren, A conceptual wing-box weight estimation model for transport aircraft, The Aeronautical Journal 117(1191) (2013) 533-551.

[6] G. Venter, J. Sobieszczanski-Sobieski, Multidisciplinary optimization of a transport aircraft wing using particle swarm optimization, Struct Multidiscip O 26(1-2) (2004) 121-131.

[7] F. Hürlimann, R. Kelm, M. Dugas, K. Oltmann, G. Kress, Mass estimation of transport aircraft wingbox structures with a CAD/CAE-based multidisciplinary process, Aerosp Sci Technol 15(4) (2011) 323-333.

[8] T. Bach, L. Heinrich, S. Dähne, C. Hühne, Structural optimization of composite wings in an automated multi-disciplinary environment, 14th AIAA Aviation Technology, Integration, and Operations Conference, 2014, p. 2295.

[9] A. Schuster, J. Scherer, T. Führer, T. Bach, D. Kohlgrüber, Automated Sizing Process of a Complete Aircraft Structure for the Usage within a MDO Process, Deutsche Gesellschaft für Luft-und Raumfahrt-Lilienthal-Oberth eV2016.

[10] P.D. Dunning, B. Stanford, H.A. Kim, Aerostructural level set topology optimization for a common research model wing, 10th AIAA Multidisciplinary Design Optimization Conference, 2014, p. 0634.

[11] S. Cumnuantip, M. Spieck, W. Krüger, An Approach for Sizing and Topology Optimization Integrating Multibody Simulation, 46th AIAA/ASME/ASCE/AHS/ASC Structures, Structural Dynamics and Materials Conference, 2005, p. 2279.

[12] B.K. Stanford, C.V. Jutte, C.A. Coker, Aeroelastic Sizing and Layout Design of a Wingbox Through Nested Optimization, Aiaa J 57(2) (2019) 848-857.

[13] C.V. Jutte, B. Stanford, C.D. Wieseman, J.B. Moore, Aeroelastic tailoring of the NASA common research model via novel material and structural configurations, 52nd aerospace sciences meeting, 2014, p. 0598.

[14] P.D. Ciampa, B. Nagel, M. Tooren, Global Local Structural Optimization of Transportation Aircraft Wings, (2010).

[15] G. Kennedy, J. Martins, A Comparison of Metallic and Composite Aircraft Wings Using Aerostructural Design Optimization, (2012).

[16] F. Dorbath, B. Nagel, V. Gollnick, Extended physics-based wing mass estimation in early design stages applying automated model generation, Proceedings of the Institution of Mechanical Engineers, Part G: Journal of Aerospace Engineering 228(7) (2013) 1010-1019.

[17] J. Qian, Automated Wingbox Structure Generation Through MATLAB, 58th AIAA/ASCE/AHS/ASC Structures, Structural Dynamics, and Materials Conference, 2017, p. 506.

[18] S.G. Kontogiannis, T. Kipouros, A.M. Savill, Multiobjective aerostructural optimization for efficient transport wing conceptual design, 2018 AIAA/ASCE/AHS/ASC Structures, Structural Dynamics, and Materials Conference, 2018, p. 0104.

[19] F. Michaud, H. Dalir, S. Joncas, Structural Design and Optimization of an Aircraft Morphing Wing: Composite Skin, J Aircraft 55(1) (2018) 195-211.

[20] G.H.C. Silva, A.P. do Prado, P.H. Cabral, R. De Breuker, J.K.S. Dillinger, Tailoring of a Composite Regional Jet Wing Using the Slice and Swap Method, J Aircraft (2019) 1-15.

[21] A. Benaouali, S. Kachel, Multidisciplinary design optimization of aircraft wing using commercial software integration, Aerosp Sci Technol 92 (2019) 766-776.

[22] K. Sinha, T. Klimmek, M. Schulze, V. Handojo, Loads analysis and structural optimization of a high aspect ratio, composite wing aircraft, CEAS Aeronautical Journal 12(2) (2021) 233-243.

[23] S. Guo, D. Li, Y. Liu, Multi-objective optimization of a composite wing subject to strength and aeroelastic constraints, Proceedings of the Institution of Mechanical Engineers, Part G: Journal of Aerospace Engineering 226(9) (2011) 1095-1106.

[24] A. Voss, T. Klimmek, Design and sizing of a parametric structural model for a UCAV configuration for loads and aeroelastic analysis, CEAS Aeronautical Journal 8(1) (2016) 67-77.

[25] K. Bramsiepe, A. Voß, T. Klimmek, Design and sizing of an aeroelastic composite model for a flying wing configuration with maneuver, gust, and landing loads, CEAS Aeronautical Journal 11(3) (2020) 677-691.

[26] F. Hürlimann, R. Kelm, M. Dugas, G. Kress, Investigation of local load introduction methods in aircraft pre-design, Aerosp Sci Technol 21(1) (2012) 31-40.

[27] F. Hürlimann, Mass Estimation of Transport Aircraft Wingbox Structures with a CAD/CAE-Based Multidisciplinary Process, ETH Zurich, 2010.

[28] L. Iorga, V. Malmedy, G. Morris, F. Albani, A. Polynkin, Large-scale optimisation for sizing of aircraft structures subject to fatigue and damage tolerance requirements, 5th Aircraft Structural Design Conference, Oct. 4-6, 2016, Manchester, England, 2016.

[29] F. Daoud, Aeroelastic shape and sizing optimization of aircraft products supported by AGILE design paradigm, 18th AIAA/ISSMO Multidisciplinary Analysis and Optimization Conference, 2017, p. 4141.

[30] S. Grihon, Structure sizing optimization capabilities at AIRBUS, World Congress of Structural and Multidisciplinary Optimisation, Springer, 2017, pp. 719-737.

[31] L.U. Hansen, P. Horst, Multilevel optimization in aircraft structural design evaluation, Comput Struct 86(1-2) (2008) 104-118.

[32] E. Valencia, V. Alulema, V. Hidalgo, D. Rodriguez, A CAD-free methodology for volume and mass properties computation of 3-D lifting surfaces and wing-box structures, Aerosp Sci Technol (2020) 106378.

[33] A. Merval, M. Samuelides, S. Grihon, Application of response surface methodology to stiffened panel optimization, 47th AIAA/ASME/ASCE/AHS/ASC Structures, Structural Dynamics, and Materials Conference 14th AIAA/ASME/AHS Adaptive Structures Conference 7th, 2006, p. 1815.

[34] W. Yang, Z. Yue, L. Li, P. Wang, Aircraft wing structural design optimization based on automated finite element modelling and ground structure approach, Eng Optimiz 48(1) (2016) 94-114.

[35] O. Dababneh, T. Kipouros, A review of aircraft wing mass estimation methods, Aerosp Sci Technol 72 (2018) 256-266.

[36] O. Dababneh, T. Kipouros, Influence of high fidelity structural models on the predicted mass of aircraft wing using design optimization, Aerosp Sci Technol 79 (2018) 164-173.

[37] C. EASA, Certification Specifications for Large Aeroplanes, February, 2009.

[38] E. Torenbeek, Development and application of a comprehensive, design-sensitive weight prediction method for wing structures of transport category aircraft, Delft University of Technology, Faculty of Aerospace Engineering, Report LR-693 (1992).

[39] J. Moran, An introduction to theoretical and computational aerodynamics, Courier Corporation2003.

[40] C. Niu, Airframe structural design: practical design information and data on aircraft structures, Conmilit Press1988.



https://dspace.org/

Identification of the key design inputs for the FEM-based preliminary sizing and mass estimation of a civil aircraft wing box structure

You, Chao; Yasaee, Mehdi; He, Shun; Yang, Daqing; Xu, Yigeng ...

2021-12-14
Elsevier
https://doi.org/10.1016/j.ast.2021.107284
You C, Yasaee M, He S, et al., (2022) Identification of the key design inputs for the FEM-based preliminary sizing and mass estimation of a civil aircraft wing box structure. Aerospace Science and Technology, Volume 121, February 2022, Article number 107284

Downloaded from a DSpace repository. https://dspace.org/